Journal of Hydrology 617 (2023) 128982

Contents lists available at ScienceDirect

Journal of Hydrology

journal homepage: www.elsevier.com/locate/jhydrol

Research papers

Assessment of sediment yield and deposition in a dry reservoir using field observations, RUSLE and remote sensing: Wadi Assarin, Oman

Mahmood M. Al-Mamari [a,*], Sameh A. Kantoush [a], Tahani M. Al-Harrasi [b], Ali Al-Maktoumi [c], Karim I. Abdrabo [a], Mohamed Saber [a], Tetsuya Sumi [a]

[a] Disaster Prevention Research Institute (DPRI), Kyoto University, Kyoto 611-0011, Japan
[b] Ministry of Agriculture, Fisheries and Water Recourses, Muscat, Oman
[c] Water Research Center, Sultan Qaboos University, Muscat, Oman

ARTICLE INFO

Keywords:
Reservoir
Sedimentation
UAV
Arid region
Wadi
Sediment delivery ratio

ABSTRACT

Soil erosion, sediment yield, and sediment transport associated with flash flooding in arid regions result in reservoir storage losses, decreased infiltration, high evaporation rates, and degradation of downstream channels. However, the lack of observational data from wadi systems and an empirical formula to compute sediment yield has hindered reservoir trapping evaluation, maintenance, and management. Therefore, this research aimed to estimate the annual soil loss in the upstream catchment area of a reservoir based on the Revised Universal Soil Loss Equation (RUSLE) with a remote sensing dataset. The sediment trapped in the Assarin Dam reservoir in Oman was estimated by coupling unmanned aerial vehicle (UAV) surveys with photogrammetry analysis to assess the reservoir siltation. Among the previous sediment trapping events, seven sets of field observation data were collected to investigate the relationship between soil loss at the catchment scale and sediment deposition volumes in the reservoir. The RUSLE method was applied to estimate soil erosion using independent factors such as rainfall erosivity, soil erodibility, topography, cover management and conservation practices. A remote sensing dataset and geographic information system (GIS) environments were used to analyse the quantitative and spatial distribution of the RUSLE parameters. Two drone surveys were conducted over the reservoir before and after a flash flood. The trapped sediment volume was estimated to be approximately 9,075 m^3 (11,343 ton) per event, representing approximately 1.26 % of the total reservoir capacity. This computed volume was validated using measurements from monitored sediment scale bars sited throughout the Assarin Dam reservoir, yielding an accuracy of 79 %. From the RUSLE results, the annual soil erosion was estimated to be 196,599 ton/ha yr^{-1}, of which approximately 5.8 % was trapped in the reservoir. Spatial-temporal variability in the rainfall patterns and the corresponding runoff discharges led to high sediment delivery at the outlet of the basin. After analysing available data from previous field surveys in Oman, a new formula for estimating the sediment yield in Wadi Assarin was developed. The results of this research, which represent the first of their type in the Middle East and North Africa (MENA) region, can support reservoir management practices and show that UAV-based photogrammetry is suitable for measuring trapped sediment volumes.

1. Introduction

Although flash floods are essential sources of groundwater recharge, they are also highly destructive natural disasters in the Middle East and North Africa (MENA) (Al-mamari et al., 2019). Therefore, retention dams have been constructed to intercept these surface flows and prevent them from draining into the sea or the desert (Abdel-Fattah et al., 2016). The critical issue associated with such dams worldwide is reservoir sedimentation, which is controlled by geological, hydraulic, and hydrological factors (George et al., 2017). In particular, high-intensity and long-duration rainfall events in arid regions cause extreme weathering of the land surface (Malmon et al., 2007), and dry environments commonly exhibit steep and bare surface landforms and landscapes, thus increasing sediment production in these regions. Moreover, flash

* Corresponding author.
E-mail addresses: almamari.mahmood.78c@st.kyoto-u.ac.jp (M.M. Al-Mamari), kantoush.samehahmed.2n@kyoto-u.ac.jp (S.A. Kantoush), tahani.alharasi@maf.gov.om (T.M. Al-Harrasi), ali4530@squ.edu.om (A. Al-Maktoumi), m.karim.ibrahim@cu.edu.eg (K.I. Abdrabo), mohamedmd.saber.3u@kyoto-u.ac.jp (M. Saber), sumi.tetsuya.2s@kyoto-u.ac.jp (T. Sumi).

https://doi.org/10.1016/j.jhydrol.2022.128982

Available online 16 December 2022

floods in dry areas can be severe and can influence sediment dynamics and sediment transport (Elçi et al., 2007).

Dam reservoirs and downstream channels suffer from several problems as a result of sedimentation, such as storage capacity losses, reservoir bed clogging, and channel degradation. Furthermore, dam conditions in arid regions differ from those in humid areas; specifically, the weathering processes resulting from high temperatures, strong winds, drought, and rainfall erosivity directly impact reservoir sedimentation. Accordingly, the soil bulk density increases with decreasing infiltration (Al-Ismaily et al., 2013). Therefore, floodwater is stored in a reservoir for only a short period (weeks) before being released to groundwater recharge downstream of the dam without considering sediment transport (Prathapar and Bawain, 2014). In Oman, the original storage capacity of the Al-Khoud Reservoir, amounting to 11.6 million cubic metres, decreased by more than 30 % due to sedimentation between 1985 and 2015 (Al-Saqri et al., 2016). Moreover, the International Commission on Large Dams (ICOLD, 2009) reported that many MENA countries will experience high reservoir sedimentation volumes by 2050. However, observed sedimentation data are unavailable in most MENA regions, many of which lack sediment gauging stations.

Consequently, measuring the amount of sediment in a reservoir is an integral component of dam operation and water resource management. Accordingly, this study aims to assess the performance of a potential sediment management technique in a wadi catchment. However, quantifying sediment yield is challenging, and our scientific understanding of sediment yields in arid environments remains incomplete due to the lack of observed data and in-depth research.

The direct and indirect techniques for measuring sedimentation in reservoirs differ from those in perennial and ephemeral streams. The typical monitoring methods of sedimentation in river systems involve bathymetric measurements using instruments such as an acoustic doppler current profiler (ADCP) and multibeam and single-beam sonar (Miranda, 2021; Asthana and Khare, 2022). In ephemeral streams, two main common monitoring techniques have been used in dry environments to estimate reservoir siltation. First, sediment scale bars have been utilized in dry reservoirs (Saber et al., 2019). These scale bars are distributed throughout a reservoir and provide local point measurements, which are then averaged and multiplied by the basin area of the reservoir to estimate the volume of trapped sediment. Second, multiple topographic surveys (using total station measurements) have been conducted to measure the amount of sediment deposited in dam reservoirs before and after floods. However, while this technique provides data on suspended and bedload materials that are more reliable and quantifiable than those from sediment scale bar surveys (Adongo et al., 2020; Shiferaw and Abebe 2021), this method requires more time and is limited to the survey area encompassing the measurement points.

Several tools have been developed to predict soil erosion and sediment yields, including sediment rating curves (Tebbi et al., 2012), numerical models, and regional sediment yield estimates (Renard and Lane, n.d.; Ghernaout and Remini 2014; Dutta 2016; Bulti 2021) and the trap efficiency of reservoirs (Brune 1953).

Understanding soil loss at the catchment scale is vital for arranging and planning mitigation structures and managing sedimentation in existing reservoirs. In an investigation into soil conservation, three main variables for soil erosion were identified (Cook 1937). This study found that the potential of rainfall erosivity, runoff and the index of soil protectivity by plant cover had a more significant impact on soil erosion. Wischmeier and Smith (1978) developed an empirical soil loss equation, the Universal Soil Loss Equation (USLE), to estimate soil erosion using erosion variable factors under specific conditions. However, a limitation of the USLE method is the prediction of the spatial distribution of soil erosion at the watershed scale. The Revised Universal Soil Loss Equation (RUSLE) developed for soil losses at the catchment scale is straightforward and applicable to integration with geographic information system (GIS) environments (Renard, 1997).

Kirurhika et al. (2011) studied soil erosion in India and found that approximately 0.16 ton/km yr^{-1} occurred; furthermore, 10 % was deposited in reservoirs, and 29 % was transported to the sea. Soil erosion prediction in arid regions is challenging due to climatic and hydrological variations. Previous research has investigated soil loss in wadi systems and found high soil erosion levels of 40 ton/km yr^{-1} using the RUSLE method (Elhag et al., 2022). Additionally, several studies have integrated the RUSLE model with high-resolution sensors to map and monitor soil erosion (Eniyew et al., 2021; Kulimushi et al., 2021).

The sediment yield in wadi channels at any location in the catchment results from soil erosion in gullies, transport, deposition and other erosion processes in the channels. The susceptibility of soil to erosion can increase due to various factors, such as soil characteristics (Ostovari et al., 2022), slope processes (Guerra et al., 2017), and drainage area (Wasson 1994), in addition to the rainfall pattern. Integrating rainfall-runoff and sediment transport models has become a principal tool for water resource assessment. However, this method depends on the data availability and hydrological responses of each subbasin according to the rainfall variability. Sediment yields in the Saudi Arabian wadi system were reported in the first model, which was derived using the general dimensional analysis method (Şen 2014).

Satellite remote sensing methods have been widely used to detect geomorphological changes in combination with field measurements, although open-source remotely sensed data typically have a coarse resolution (Yousefi et al., 2021). In recent years, the ground-based LiDAR technique has been widely used with high accuracy to generate digital elevation models (DEMs) or scan 3D objects in combination with photogrammetry analysis. However, the LiDAR technique is costly and more effective for local-scale investigations (Rogers et al., 2020). The use of unmanned aerial systems (UASs) with photogrammetry analysis can yield high spatial coverage, good accessibility, and high accuracy (Salach et al., 2018). These concepts vary depending on the condition and scale of the research area. Developments in remote sensing have led to relatively inexpensive and rapidly deployable devices such as unmanned aerial vehicles (UAVs), with which erosion and deposition processes can be mapped and quantified at increasingly fine spatial resolutions. At present, empirical algorithms are continuously being transferred from existing remote sensing technologies to UAVs. Considering that monitoring and investigating the transport of sediment require accurate, high-resolution spatial data representing the Earth's surface (Clapuyt et al., 2016), UAVs (also called drones) and photogrammetric processing techniques allow very high-resolution river data to be acquired nearly effortlessly. Other geoscientific applications of photogrammetry techniques include the detection of fluvial changes in a river system (Tamminga et al., 2015) and geomorphic observations of a landslide (Tsunetaka et al., 2020). Combining these techniques could provide an economical and rapid solution for monitoring reservoir sedimentation in arid regions.

Therefore, this research aimed to estimate soil loss upstream of a reservoir catchment using the RUSLE approach and its association with trapped sediment in the reservoir. The volume of sediment trapped in a dam reservoir was quantified with acceptable and representative values by using multitemporal drone and field surveys combined with photogrammetric analysis, with the total volume of sedimentation being estimated using the level of sediment measured with sediment scale bars. The workflow of the multitemporal topographic surveys conducted herein required the acquisition of considerable data and the implementation of numerous postprocessing steps. Finally, a sediment yield formula is proposed based on an analysis of the available data.

2. Study area

The study area is the Assarin Dam located southeast of Muscat (2571416.15 m N, 660927.40 m E), the capital of Oman (Fig. 1). The Assarin Dam was constructed in 2011 after an extreme tropical cyclone named Gonu caused severe damage to the infrastructure and property in the region. Usually, dams in wadi systems are built for multiple

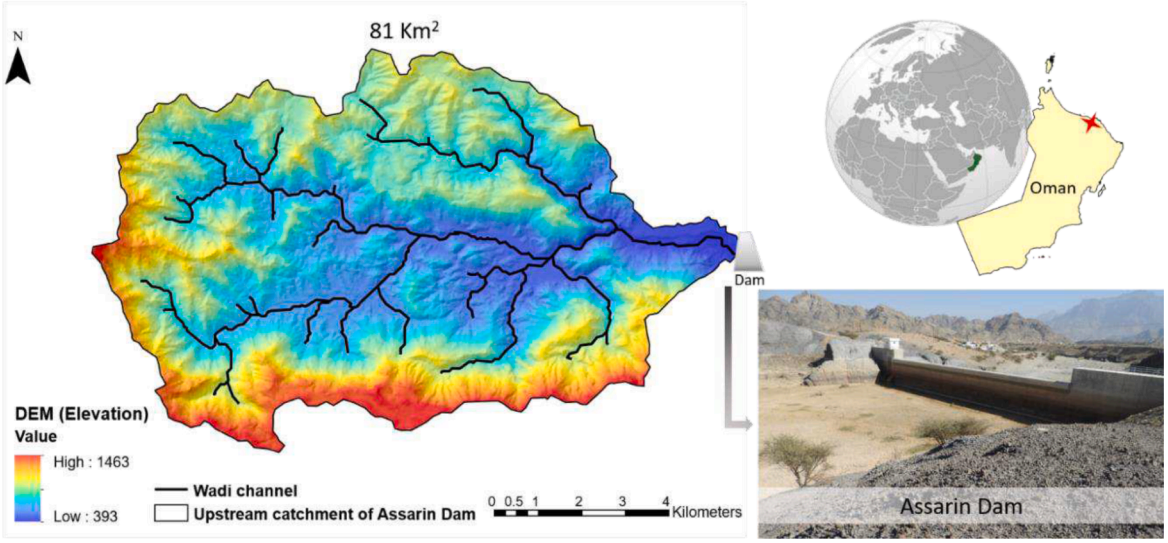

Fig. 1. The catchment area of the Assarin Dam, showing the topographic elevation.

functions, such as flood control, groundwater recharge, and water storage. The Assarin Dam reservoir has a capacity of 0.72 million cubic metres and a catchment area of 81 km^2 (8,100 ha) (Ministry of Regional Municipalities & Water, 2012). The catchment is geologically underlain by numerous sedimentary rock formations and features a valley with steep slopes at elevations ranging from 1000 m to more than 1300 m above the mean sea level (Moraetis et al., 2020). In Oman, sediments trapped in dam reservoirs are irregularly removed by excavation without measurement or monitoring systems. Within the upstream catchment of the dam reservoir, no monitoring data were available; therefore, precipitation satellite data were used.

3. Materials and methodology

The methodology combined different approaches from field measurements, remote sensing analysis, hydrological, and RUSLE models to assess reservoir siltation and estimate the sediment yield from the catchment in the wadi basin. Fig. 2 shows the proposed flowchart of the detailed methodological approaches suitable for the wadi basins in arid areas. Further details for each approach are described in the following subsections. For instance, in section 3.1, the RUSLE and five different factors – namely, rainfall erosivity (R), soil erodibility (K), slope length and steepness (LS), cover management (C), and practice management (P) – are introduced to estimate the average annual soil erosion in the catchment. Additionally, a field investigation and drone survey were performed to understand the reservoir siltation and quantify the sediment yield as described in sections 3.2, 3.3, and 3.4. Moreover, the extreme events that caused flash floods and transported sediment deposited in the reservoir were computed. Finally, the sediment delivery ratio is determined from the sediment measured from the field surveys, and the gross erosion per unit area is calculated with the RUSLE.

3.1. RUSLE

The RUSLE method to predict soil erosion has been widely used for estimating annual soil loss at the watershed scale using independent factors. Based on the GASEMT database, approximately 507 studies and investigations have used the RUSLE method (Borrelli et al., 2021). The

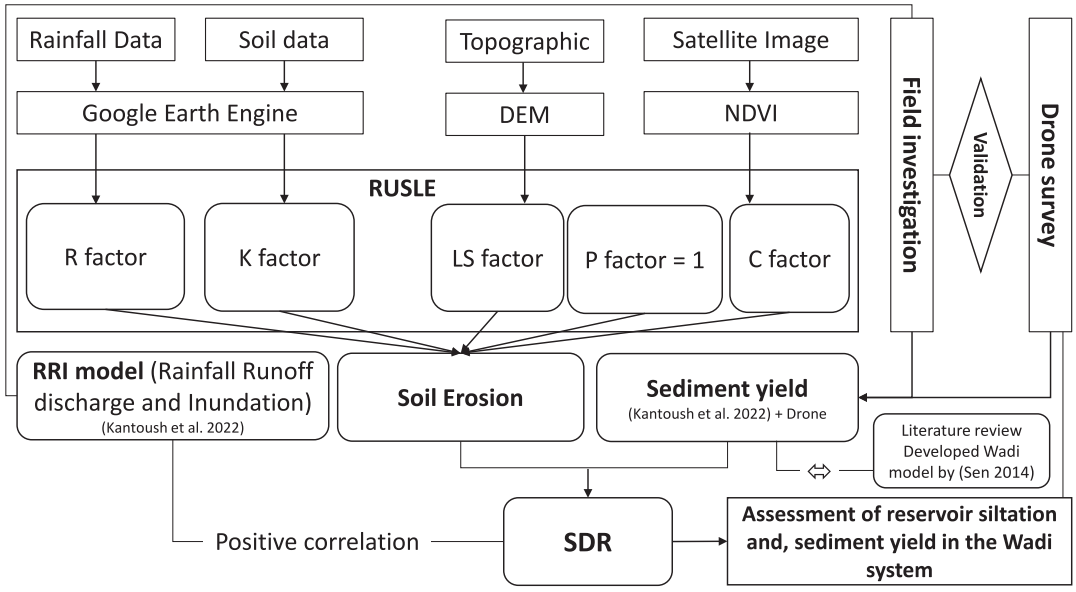

Fig. 2. Flow chart of the overall methodology to assess reservoir siltation and sediment yield in a wadi system.

RUSLE has been used in various dry environments, such as Jordan (Farhan and Nawaiseh, 2015), Egypt (Elnashar et al., 2021), Algeria (Melalih and Mazour, 2021), and Iraq and Iran (Allafta and Opp, 2022). The RUSLE equation yields the soil erosion per unit area in unit time, which is expressed as:

$$A = RKLSCP \quad (1)$$

where R is the rainfall erosivity factor (MJ mm h^{-1} ha^{-1} yr^{-1}), K is the soil erodibility factor (ton ha h/ha MJ^{-1} mm^{-1}), LS is the slope length and steepness factor (dimensionless), C is the cover management factor and P is the conservation practice (dimensionless), all of which are factors used for the estimation of the average annual soil loss (A) (ton/ha yr^{-1}). The raster layers of rainfall erosivity and soil erodibility were calculated and extracted from the Google Earth Engine (GEE) (Wang and Zhao, 2020; Islam, 2022).

3.1.1. Data sources and processing

3.1.1.1. Rainfall erosivity factor (R). Due to the lack of observed hydrological data and the nonhomogeneous spatial distributions of ground stations in most of the wadi systems in arid environments, a satellite precipitation dataset was used to determine the rainfall erosivity. Therefore, the monthly precipitation dataset with a downscaled 1.0 km^2 resolution from SM2RAIN-ASCAT was applied to calculate the R factor over the catchment area in Eq. (2) (Wischmeier and Smith, 1978).

$$R = 1.73*10^{\left(1.5*log\left(\frac{P_m^2}{P_a}\right)-0.08188\right)} \quad (2)$$

where R is the rainfall erosivity in MJ mm $ha^{-1}h^{-1}$ yr^{-1}, P_m is the monthly precipitation (mm) and P_a is the yearly precipitation (mm). The accuracy of the satellite precipitation dataset was investigated and tested with regional observation data in Iran, which neighbours Oman to the north, and the results showed that SM2RAIN-ASCAT had better accuracy than PERSIAN-CCS and CMORPH, with root square mean errors (RMSEs) of 2.4 mm, 4.36 mm and 28.83 mm, respectively (Eini et al., 2021).

The annual average rainfall in the reservoir catchment was 104 mm. In total, seven significant flood events were recorded in Wadi Assarin from 2011 to 2019, ranging from 27.4 to 134.4 mm, with rainfall intensities ranging from 2.6 to 6.7 mm/hr (at the nearest available gauge station to the catchment) (Fig. 10a). These rainfall intensities over bare land in arid regions cause high erosivity due to the kinetic energy of raindrops. Additionally, the shear stress induced by flash floods passing over dry channel beds increases sediment transport from the drainage network to the reservoir (Azab et al., 2021). The available data from the surrounding catchments demonstrate that the reservoir in the Wadi Assarin is exposed to one extreme flash flood per year, which was confirmed by pedon analysis.

3.1.1.2. Soil erodibility (K). The K factor represents the resistance of soil to erosion from the impacts of kinetic energy from raindrops. This factor depends on the soil structure, texture, organic content, and porosity. The SoilGrids250 m dataset was used to estimate the soil texture (sand, clay and silt content) and organic carbon content to compute the K factor using Eq. (3) (Sharpley and Williams 1990; Hengl et al., 2017)

$$K = \left[0.2+0.3*exp-0.0256*SAN*\left(\frac{1-SIL}{100}\right)\right]*\left[1-\frac{0.25*CLA}{CLA+exp(3.72-2.95*CLA)}\right] \quad (3)$$

where SAN, SIL and CLA are the percentages of sand, silt and clay (%), respectively. The K factor was calculated using Eq. (3) in GEE.

3.1.1.3. Topography factor (LS). The LS factor represents the topographical effect on soil erosion based on slope length and steepness, which can accelerate the effects of rainfall. The LS factor includes the flow accumulation and slope degree determined from the DEM with a 5-metre resolution (National Survey Authority-Oman). The LS was calculated using Eq. (4) (Moore et al., 1991).

$$LS = (0.4+1)*\left(\frac{Flowaccmulation*Cellsize}{22.13}\right)^{0.4}*\left(\frac{sin(slope)}{0.0896}\right)^{1.3} \quad (4)$$

where L and S describe slope length and steepness (dimensionless), flow accumulation represents the cumulative upslope of cells that contribute to flow for a particular cell, cell size equals the size of the grid cell, and sine slope equals the sin of the slope angle (in degrees).

3.1.1.4. Cover management factor (C). The impacts of land cover and plant management upstream of the reservoir catchment are very limited. The NDVI was obtained from Landsat-8 satellite images using red and near-infrared wavebands, and the C factor was estimated with the following equation (Durigon et al., 2014):

$$C = 0.1*\left(\frac{(-NDVI+1)}{2}\right) \quad (5)$$

where NDVI is the normalized difference vegetation index.

3.1.1.4.1. Management practice factor (P). Overall, no central conservation practice in the target study area affects the hydrodynamics of flash floods. In previous research, a P value of 1 was assumed for all watersheds in arid regions (Gaubi et al., 2017).

3.2. Sediment yield-runoff relationship in the wadi system

Developing empirical approaches and charts for specific conditions and regions is essential for obtaining and understanding these phenomena. The lack of observational data is the major challenge in evaluating the sediment yield in arid regions. Kantoush et al. (2022) conducted field surveys to estimate the trapped sediments in the Assarin Dam reservoir for different periods using the sediment scale bar and GIS environments. The discharge of the watershed was simulated by using the rainfall–runoff–inundation (RRI) model without dams to calibrate and validate the model with the downstream gauging station. Their results, which included drone measurements, were compared with predicted sediment yield values from the sediment yield model developed by Şen (2014) for another wadi system. The empirical model in Eq. (6) was used only for comparative purposes. The model identified and analysed the sediment yield in the wadi system using physical relations and the calculation of some correlated variables in the catchment with homogeneous dimensions. The four most significant variables were selected to develop the following sediment yield equation:

$$S_y = 0.0001*S*\frac{Q}{A} \quad (6)$$

where S_y is the sediment yield, S is the mean channel slope (dimensionless), Q is the discharge (m^3/s), and A is the catchment area (km^2). The sediment yield was estimated for several subcatchments upstream of the Wadi Jizan dam in southwestern Saudi Arabia.

3.3. Field survey and photogrammetry

In this study, field and drone surveys were conducted to estimate the volume of sediment trapped in a wadi system reservoir in an arid region. The spillway and sluice gate of the Assarin Dam are located in the high stage, which reduces the vulnerability of fine and coarse sediment transport from the reservoir to the downstream channel. Additionally, the water was stored in the reservoir for more than two weeks before being released downstream to promote the groundwater recharge process. The flash flood that occurred between field surveys in the Wadi Assarin filled the dam reservoir without a spillway. Therefore, it can be assumed that the trapped sediment is equal to the sediment yield. A total of 19 sediment scale bars (pegs) were installed throughout the reservoir based on the bed elevation to measure sediment deposition during the construction of the Assarin Dam (Fig. 3**b**). The sediment scale bars were installed with two different post heights: eleven bars located near the dam have a height of 1.5 m, while the other 8 bars have a height of 1 m. To investigate the siltation in the reservoir and determine the sediment volume, two drone surveys were conducted in the dam reservoir: one on 17 March 2019, yielding 223 images, and one on 25 August 2019, yielding 430 images. The readings from sediment scale bars reveal the variance in the distribution of sediment deposits across the reservoir due to previous flash floods, which eroded the reservoir bed before the sediments were retained by the dam body. Fig. 3**a** shows the sediment bar readings obtained in two periods (before and after a flood event) and their corresponding locations throughout the dam reservoir.

A total of 15 ground control points (GCPs) were sited around the study area at different elevations on stable topographic formations (e.g., painted hard rocks) (Fig. 3**b**). The GCPs were measured by real-time kinematic global navigation satellite system (RTK-GNSS) receivers combined with Leica Viva GS14 and Leica Viva CS15 field controllers (Fig. 3). The horizontal and vertical accuracies of the RTK-GNSS positioning data were approximately 0.01 m and 0.02 m, respectively.

Moreover, three reference marks postdating the construction of the dam were used in the photogrammetric analysis. A DJI Phantom 4 camera with a resolution of 5472 × 3648 pixels was used to acquire overhead aerial photographs. In this research, drone missions were conducted over the reservoir during two field surveys in March 2019 and August 2019. A flash flood occurred between these field surveys, enabling us to detect and quantify the changes induced by the sediment deposited during the event using image-based techniques with UAV-derived and scale bar-measured values. The drone maintained an average altitude of 80 m above the ground surface during flight. Most of the acquired images were considered to have covered each GCP at least twice. In this application, two approaches were utilized to quantify and measure the volume of trapped sediment. First, inverse distance weighting (IDW) interpolation was used to generate raster layers by comparing the sediment scale values collected during the two field surveys with the DEMs generated via photogrammetric processing. IDW interpolation, which depends on a linear combination of weighted distance samples, has been reported to be reliably accurate (Rishikeshan et al., 2014; Polat, Uysal, and Toprak 2015; Arseni et al., 2019). The measurements from the nineteen sediment scale bars were input to apply IDW interpolation to the selected polygons for the dam reservoir using the Spatial Analyst toolbox in ArcGIS 10.8.

Second, the images acquired in the two survey periods were analysed using the commercial software product Agisoft Metashape. Initially, all high-accuracy photos were aligned based on the register alignment received from the simultaneity of a Global Positioning System (GPS) device in the UAV with the default settings, namely, a key point limit of 40,000 and a tie point limit of 4000. The alignment settings were chosen from the Agisoft Metashape Professional User Manual (version 1.6.5) with the spatial accuracy increasing from 10 to 1000 m. These parameters were selected based on the investigations performed by Nesbit (Nesbit and Hugenholtz, 2019) for high-relief landscapes. The collected GCP data were imported and relocated to correct erroneous changes, and the cameras were calibrated to the original georeferenced data by using the 'optimize cameras' function. Then, dense point clouds were generated using high-quality, aggressive depth filtering, which previous research has conclusively shown improves the point cloud data density (Tinkham and Swayze, 2021), and previous studies have indicated that various point cloud density parameters significantly impact the quality of the results. In this study, the dense point cloud model was constructed based on overlapping images (>50 % with the distance between images ranging from 10 to 20 m) capable of recognizing matching points (tie points). Finally, DEMs were generated for March 2019 and August 2019 from the dense point clouds at resolutions of 0.09 m and 0.03 m per pixel, respectively. The reservoir zone was extracted using a similar boundary layer and cell resolution (0.09 m pixel) to identify the geomorphological changes between the two survey periods (Fig. 3).

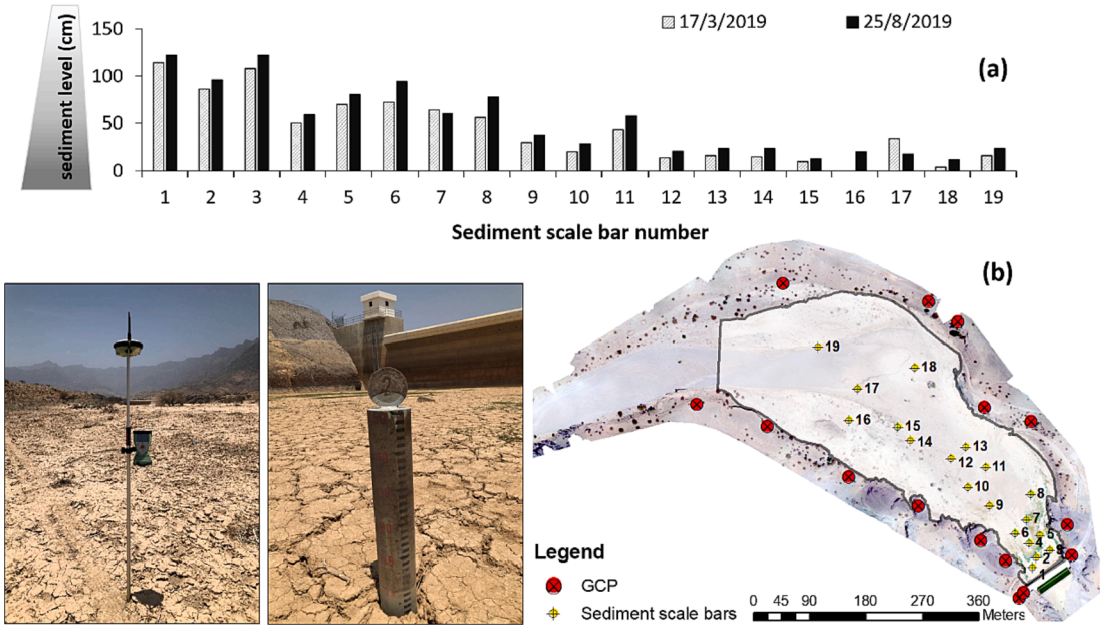

Fig. 3. (a) Sediment level values measured in the dam reservoir and (b) sediment scale bar locations and ground control points.

Table 1
Reservoir sedimentation for seven flood events in the Wadi Assarin.

Flood events		Deposited Sediment volume [m^3]	Deposited sediment weight [ton]
Date	Year		
Nov 12	2012	4,405	5,506
Apr 13	2013	3,975	4,969
Oct 15	2015	3,511	4,389
Mar 16	2016	3,165	3,956
Dec 17	2017	6,274	7,843
Oct 18	2018	5,783	7,229
May 19	2019	9,075	11,343

Seven flash flood events and associated siltation in the reservoir were conducted to assess the interrelation between sediment yield, rainfall intensity and flow discharges. Several monitoring techniques were used for quantifying reservoir sedimentation volumes, which were reported by Kantoush et al. (2022) and based on UAV photogrammetry and sediment scale bars before and after floods. Table 1 summarizes the dates of the flash flood events and computed sediment deposited volumes and weight considering the sediment bulk density of 1,250 kg/m^3.

3.4. Data postprocessing

Large volumes of nutrients and debris are transported in floodwaters and settle in dam reservoirs. Therefore, vegetation (such as small shrubs) is common in reservoir areas, resulting in a point cloud that poorly represents the surface. In this study, image analysis functions were used to remove unwanted objects (including vegetation) from the generated DEMs by computing the normalized difference vegetation index (NDVI) and using the results to identify shrubs in aerial photos. Then, a masking function was applied to exclude pixels containing NDVI values within a defined range from the DEMs. Finally, the pixels containing 'no data' in the DEMs were filled based on a combination of plane-fitting and IDW interpolation techniques with extensive interpolation by using the 'Elevation Void Fill' function (Raster Function Template Editor) in ArcGIS 10.8. As an alternative, we tested the classification option in Agisoft Photoscan by removing the vegetation cover from the dense point cloud before the DEMs were generated, and similar results were obtained. In this method, we used the mask shape created by the NDVI to classify the dense point clouds by shape.

After completing these steps, DEMs of differences (DoDs) were used to quantify the volume of sediment trapped in the dam reservoir. The basic concept of this method involves differencing the georeferenced DEMs obtained in two different periods, with the resulting raster

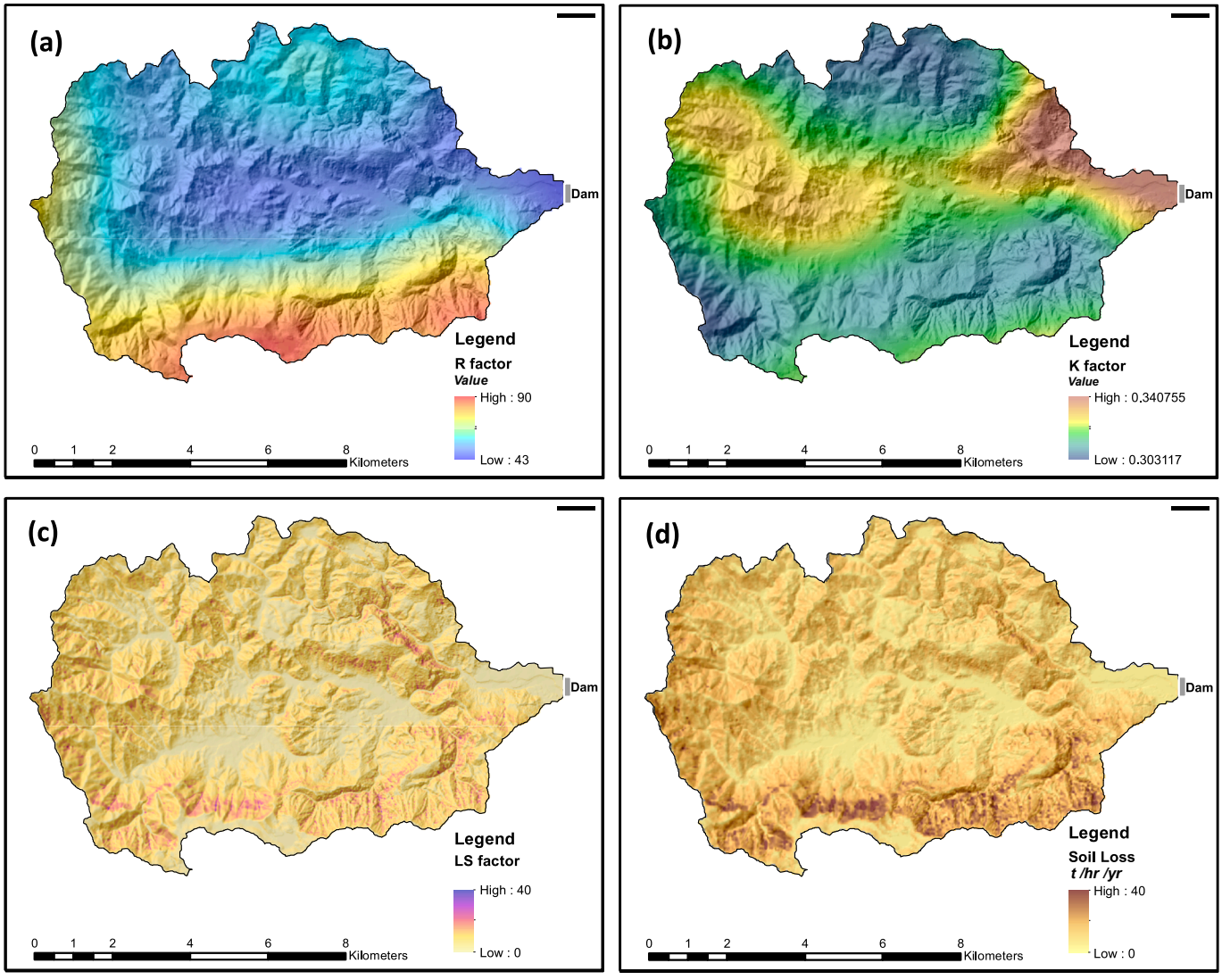

Fig. 4. Spatial variation in (a) rainfall erosivity, R factor (MJ mm $ha^{-1}h^{-1}$ yr^{-1}), (b) soil erodibility, K factor (ton ha h/ha MJ^{-1} mm^{-1}), (c) slope length steepness, LS factor, and (d) annual soil loss (ton/ha yr^{-1}).

representing the morphological changes between the two periods (Cândido et al., 2020). The total volume of sediment was computed by multiplying the deposit thickness by the pixel area.

4. Results

4.1. Estimated soil loss

The R factor is a function of the distribution of the annual rainfall. The minimum and maximum R values were 43 and 90 MJ mm ha^{-1} yr^{-1}, respectively (Fig. 4a). A higher R value was present at high and steep topography in the southern part of the catchment. Fig. 4b shows that the K factor ranged from 0.30 to 0.34, with a mean value of 0.32. The highest soil erodibility was found near the downstream area and along the central part of the catchment, which corresponds to the sedimentary surface. The distribution of the LS factor ranged from 0 to 40, and the LS value was higher in the southern and northeastern parts of the catchment (Fig. 4c). The contribution of the C factor to soil erosion was very minimal, with values between 0.042 and 0.052, because the study area is mountainous and is located in the uppermost parts of the basin. The soil loss map showed a high correspondence to the pattern of the R and LS factor maps (Fig. 4d). The slope steepness and length were responsible for increasing the overland runoff and concentration time, thereby increasing soil erosion. The computed soil loss in the Assarin catchment ranged from zero in the plain area to over 40 ton/ha yr^{-1}, with an average annual soil loss of approximately 19,6599 ton/ha yr^{-1}. The soil erosion scale upstream of the reservoir catchment was very severe compared to the catchment size. Therefore, the implementation of conservation measures is required in efforts to reduce the erosion process in such areas. Moreover, the selection of suitable sites for dam locations should be considered nearest to the production source of sediment in such mountainous areas of arid regions.

4.2. Estimated sediment delivery ratio (SDR)

The field measurement data of trapped sediment in the reservoir can be exploited to investigate the relationship between soil erosion and sediment delivery in the basin. Therefore, the SDR values were determined based on the ratio between a different observed scale of sediment yield data and the annual averaged soil loss. The SDR of the upstream reservoir catchment varied from 0.020 to 0.058, with an average of 0.033. Indeed, the sediment delivery strongly corresponded to the hydrological runoff processes in the catchment. Fig. 5 shows a linear relationship between the SDR and the total discharge with a strong positive coefficient of correlation (R^2) equal to 0.88. As a result, the effective runoff is responsible for transporting large amounts of eroded soil from the eroding portions of the catchment to the outlet (sediment yield).

4.3. IDW and DEM uncertainties

IDW analysis depends mainly on the sample value density and distribution in the target area to represent the morphological changes. However, the primary source of IDW uncertainty in this study was the resolution of the scale bars in the dam reservoir. On the other hand, photogrammetric analysis based on UAV-derived images was conducted with dense point clouds containing more than 45 million data points, and DEMs were generated for both periods using the workflow shown in Fig. 6.

The DEMs representing both periods were extracted at a 0.09-m resolution. The two drone surveys had only minor differences with regard to their spatial coverage, their view of the outer periphery of the study area, and their distance from the target zones (Fig. 7). The orthomosaic photographs demonstrate that some zones in the main channel were scoured and affected by flash floods in March 2019, as shown in Fig. 7a. This process occurred during low discharge, at which time sediment that had been transported during the previous event settled in the deltaic area upstream of the dam. Additionally, the drone surveys showed the area of excavated sediments that farmers used for agricultural practices (Fig. 7b). During the field survey, we found depression springs near the dam structure; these springs eroded nearby sediments at depths of 10 to 15 cm (one instance of which is shown in Fig. 8a). Moreover, the exposed terrain surface of the dam reservoir following drying was impacted by extreme weathering, causing the sediment to consolidate and resulting in cracking and high bulk densities, as shown in Fig. 8b and 8c.

The uncertainties on the x-, y-, and z-axes in the photogrammetric results were calculated using the analysis tools in Agisoft Photoscan. The average errors derived from the root mean square error (RMSE) were approximately 8 and 6 mm for the GCP z-axes in March 2019 and August 2019, respectively. However, some errors occurred due to the lack of GCPs in the centre of the reservoir. The RMSEs obtained at the GCP locations and the error estimates for the x-, y-, and z-axes are shown in Table 2.

4.4. Digital elevation model of differences (DoD)

The volumetric change in trapped sediment was detected using multiple overlapping DEMs by determining the changes in elevation for the same pixels in the reservoir bed between the two periods. The DoD algorithm was processed in a raster calculator in ArcMap 10.8 to measure the morphological changes between the data obtained in the two survey periods. Additionally, the Geomorphic Change Detection Tool (GCD v7.2) was used to detect the variations between the two DEMs (Wheaton et al., 2009; Özcan and Özcan 2021). In this study, DEMs were generated for the two field surveys included in this analysis to estimate the volumes of trapped sediment with an identical cell resolution (0.09 m) using Esri's ArcGIS (Fig. 9). DoDs were then computed from these generated DEMs by subtracting $DEM_{Aug.2019}$ from $DEM_{Mar.2019}$ (generated DEMs pre- and postflood with the same extent) to estimate the net change in the sediment volume.

The total volume of trapped sediment obtained by the structure from motion (SfM) technique (9075 m^3) was higher than that obtained by the conventional method (7688 m^3) mentioned previously in the

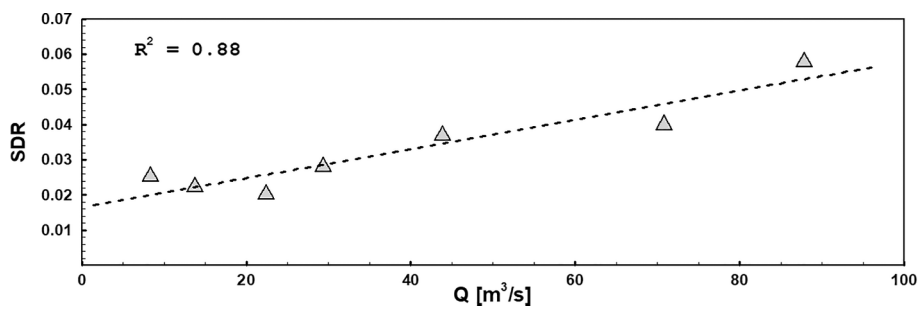

Fig. 5. The relationship between the sediment delivery ratio and discharge in the Wadi Assarin.

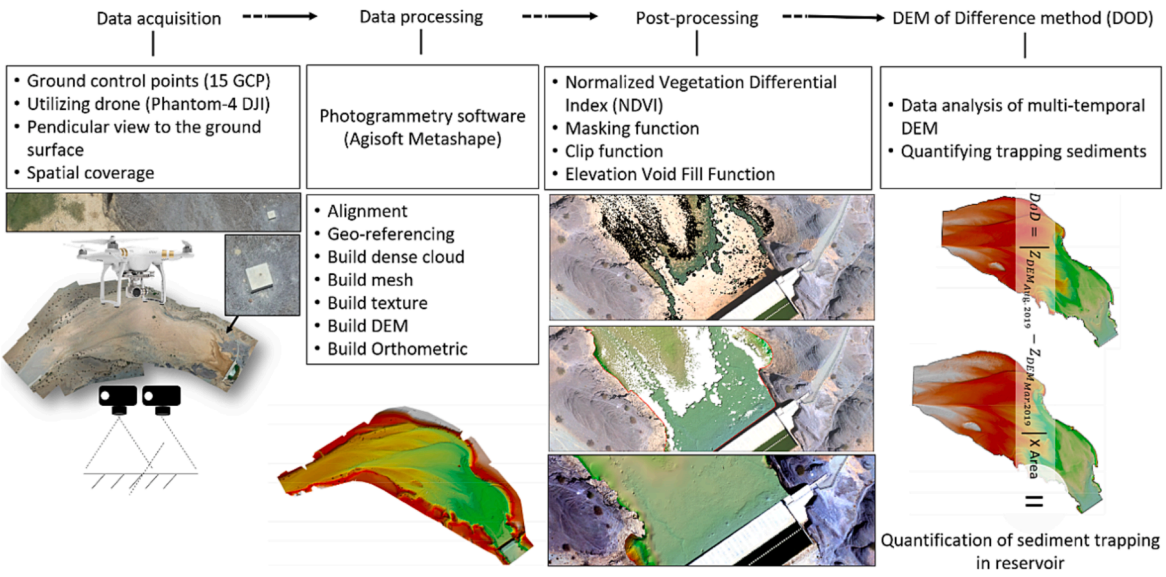

Fig. 6. Processing flow chart showing the generation of multiperiod DEMs.

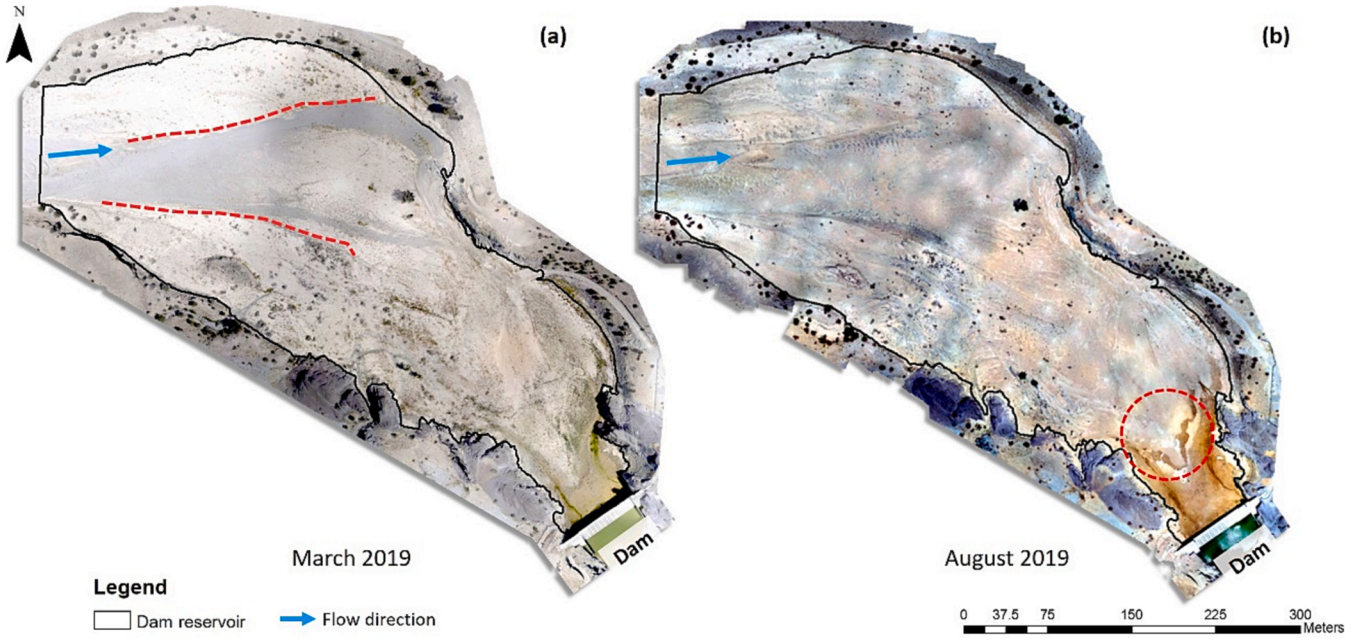

Fig. 7. (a) Aerial photo of the drone survey conducted in March 2019 (the red line denotes the delta formation) and (b) aerial photo of the drone survey conducted in August 2019 (the red circle denotes the excavation area). (For interpretation of the references to colour in this figure legend, the reader is referred to the web version of this article.)

Introduction. The IDW interpolation result was computed to be 10829 m^3 without considering erosion effects. Comparing the results obtained with the DoD and IDW approaches reveals that both methods yielded similar ranges for the estimated volume of trapped sediment. However, a possible explanation for these results is that the scale bar levels were interpolated (with IDW) from a homogeneous elevation, whereas in reality, all the measured elevations varied. Therefore, the IDW results should be considerably different from the volumes of trapped sediment measured by the drone surveys. These measurements were produced following a rainfall event with a mean rainfall intensity of 6.7 mm/hr.

4.5. Validation of DoDs

This study's procedures were validated by comparing the differences in the measured sediment elevations between the two periods with those at the same measurement points in the generated DEMs (Fig. 10a). The maximum elevation difference was 3 cm among the 19 scale bar sites distributed throughout the dam reservoir. Additionally, a significant positive correlation (R^2 = 0.82) was found between the sediment elevation changes measured by the sediment scale bars and those determined using the SfM technique (Fig. 10b).

The scale of sediment accumulation and the rapid increase in sediment deposition near the dam are serious problems that cause the reservoir capacity to drop instantaneously, reducing the dam's ability to retain floodwater and protect downstream areas, resulting in degradation of the downstream channel bed. Indeed, the morphological characteristics of the reservoir bed should be considered in wadi systems due to the important impacts of the sediment distribution on the efficacy of

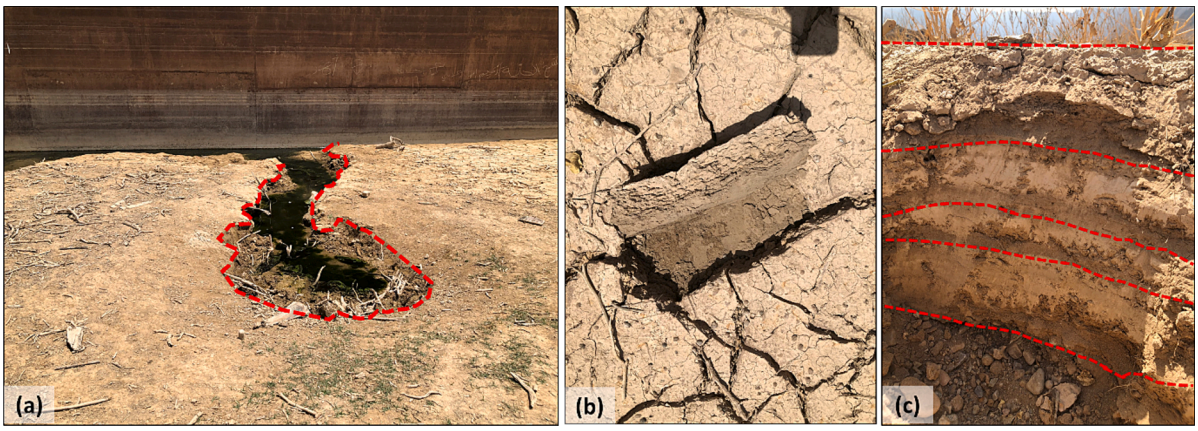

Fig. 8. (a) Sediment erosion caused by depression springs. (b, c) dried-out silty layer with cracks and high bulk density.

Table 2
Ground control point RMSEs.

GCP	X error (cm)	Y error (cm)	Z error (cm)
Mar.2019	1.53	1.09	0.64
Aug.2019	3.73	3.05	0.87

flood mitigation structures and reservoir capacities.

As shown in cross-sections 1 and 2, a large volume of sediment accumulated on the left side of the reservoir due to differences in elevation and flow in the main channel that occurred during the rising phase of the flash flood (Fig. 11**C1, C2**). These sediment deposits were between approximately 10 and 25 cm thick. However, cross-sections 3 and 4 show the erosion process in the upstream area of the reservoir,

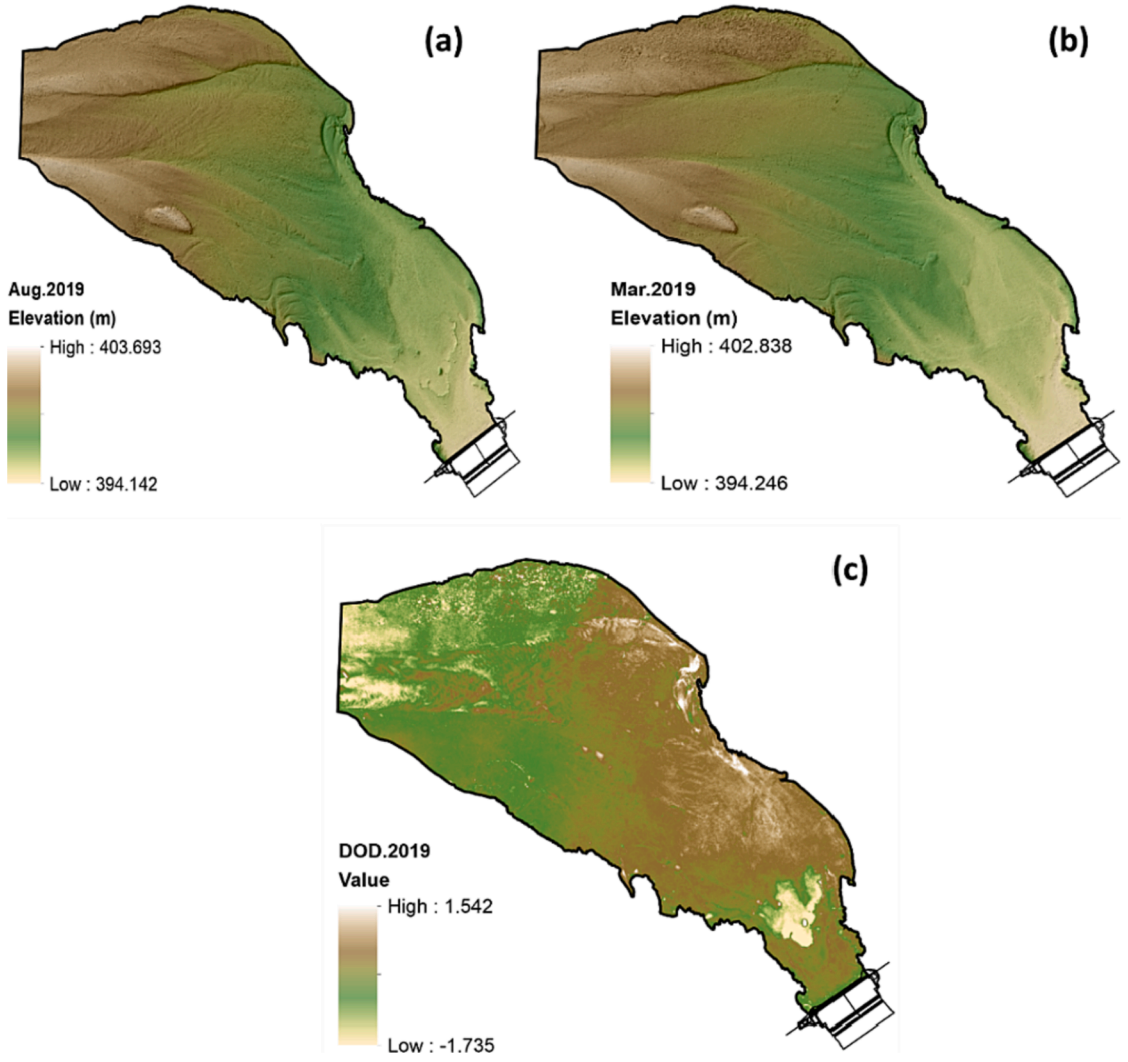

Fig. 9. (a) DEM generated for August 2019; (b) DEM generated for March 2019; and (c) DEM of difference (DoD).

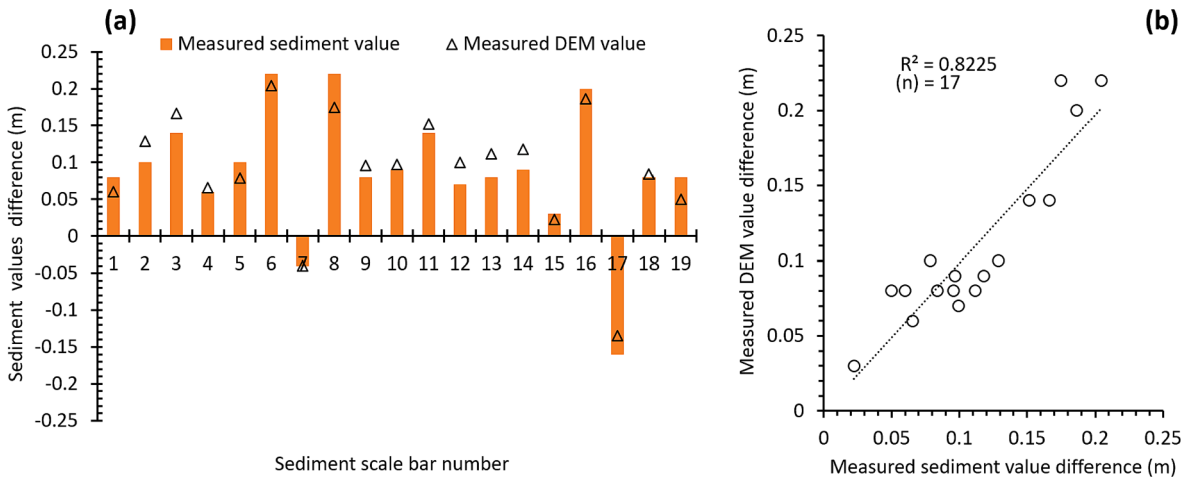

Fig. 10. (a) Comparison between the sediment scale bar value and DEM value differences and (b) correlation between the observed measurement values and processed DEM values.

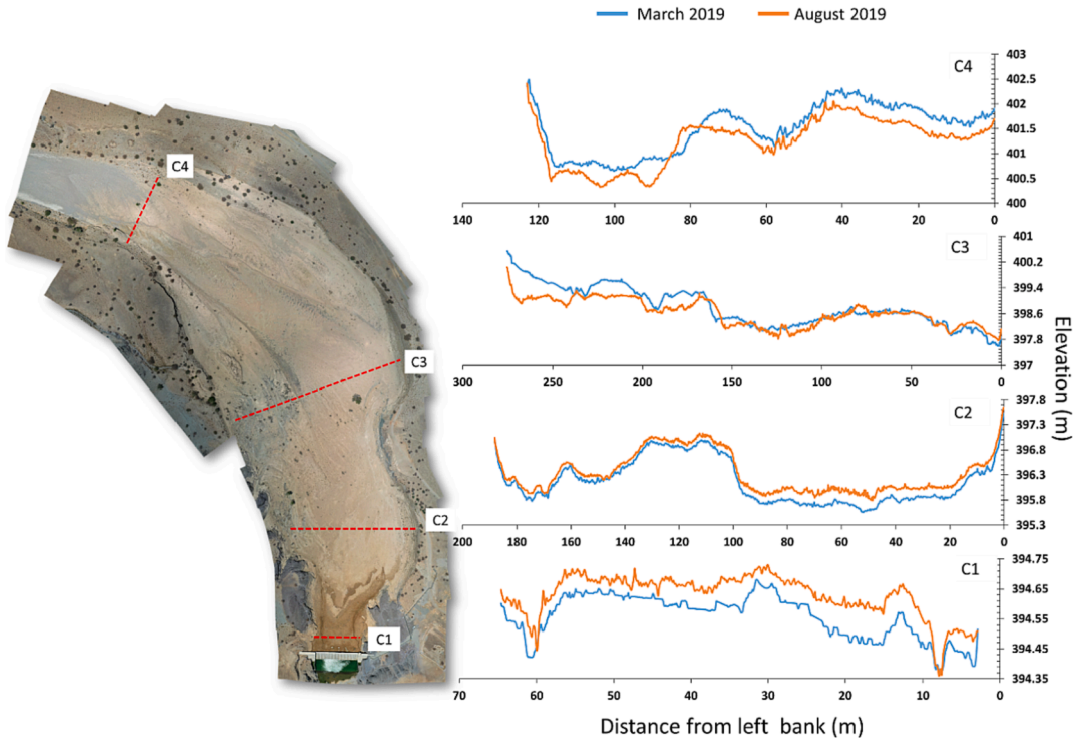

Fig. 11. Comparison of the cross-sections generated from the DEMs representing March and August 2019.

which may have also been affected by the rising phase of the flash flood (Fig. 11**C3, C4**). Additionally, cross-section 1 shows smaller erosion zones on both sides of the cross-section that were eroded by the water released from the dam reservoir. Moreover, the meandering channel upstream of the dam experienced increased sediment erosion, and the sediments from this channel were later deposited close to the dam. Saber et al. (2022) conducted pedon analysis in the Assarin Dam using the hydrometer method. He found that in 2 pedons near the dam, the soil texture of the top 1st layer was silty followed by a coarse sandy loam layer with a bulk density of approximately 1,250 kg/m^3.

These findings suggest that drone surveys can be used to construct and inspect sediment elevation curves representing reservoir sedimentation by using data from surveys conducted before and after storms that cause flash floods. In this study, we estimated the volume of sediment trapped in the Wadi Assarin catchment in 2019. Quantifying the volume of trapped sediment can help explain complex sediment transport mechanisms in catchments.

5. Discussion

5.1. Sediment yield in relation to rainfall intensity

Quantifying the sediment yield in wadi systems based on monitoring and modelling methods is limited in previous research studies. The sediment depth thickness measured from the March 2019 survey represents the total sediment deposition in the dam reservoir since the dam was constructed in 2011, which is equal to the values reported by Kantoush et al. (2022). The trapped sediment volume based on the sediment scale bar level and IDW method between the March 2019 survey and the original reservoir bed was estimated to be approximately

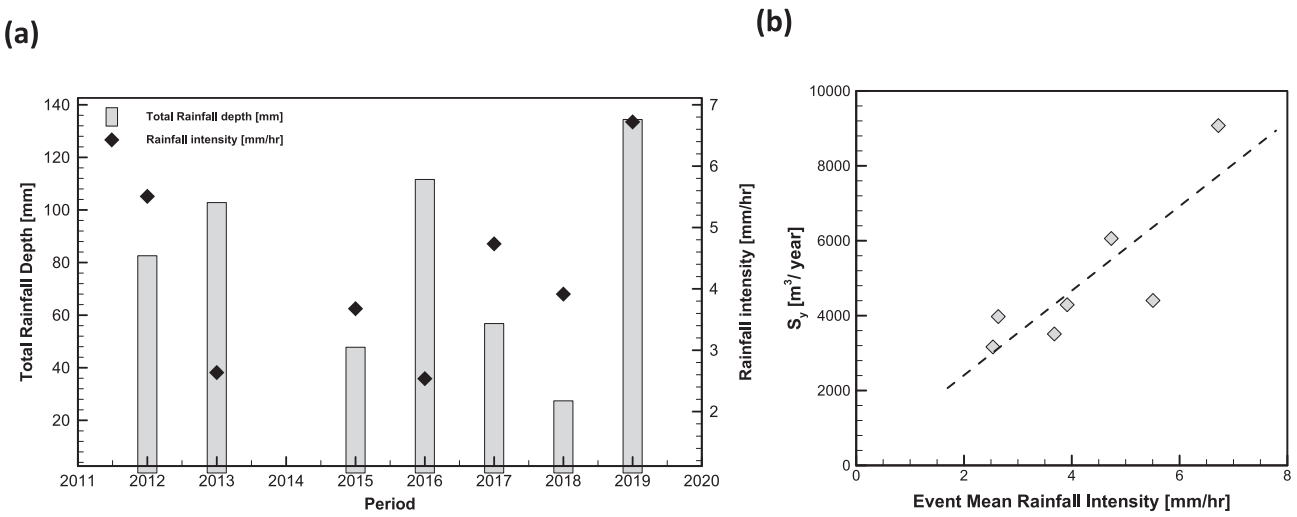

Fig. 12. (a) The available data of total rainfall depths with rainfall intensity. (b) Relationship between sediment yield and rainfall intensity in the Wadi Assarin.

36,270 m^3. The flash flood magnitude in the dry wadi channel reflects the rainfall regime. Fig. 12a shows the rainfall depth values and their corresponding intensities for event durations. The available rainfall data showed that rainfall intensities higher than 4 mm/hr caused a large amount of erosion and sediment transport. Conversely, rainfall intensities ranging between 2.5 and 3.7 mm/hr produced low sediment yields. The sediment yield increased with increasing rainfall intensity (Fig. 12b). The temporal variation in the intensity of different events is a major factor that impacts the sediment yield in dry environments. It has been demonstrated that soil loss increases as the intensity increases from 3 to 5 mm/hr (Ziadat and Taimeh 2013). Fig. 12b shows a positive correlation between the generated sediment yield and the effectiveness of rainfall intensity. The soil lost from the watershed due to erosion is transported through the drainage network and temporarily deposited in various stages and locations. The estimated annual soil losses from the reservoir watershed equal 196,599 ton/ha yr^{-1}, of which approximately 5.8 % is trapped in the reservoir based on the drone measurements, and 94.0 % of the eroded sediment is redeposited in the basin. These trapped sediments accumulate over time with the occurrence of flood events.

5.2. Sediment yield in relation to runoff–flow discharge

The hydrological responses in the Assarin watershed under various rainfall intensities, runoff levels, and sediment yields were collected over 7 years of monitoring. The seven years of existing measured values for the trapped sediments in the Assarin reservoir and the runoff discharge were positively correlated with an R^2 equal to 0.8. Normally, obtaining a correlation between runoff discharge and sediment yield during a flood is challenging, especially in arid regions. The sediment yield data show a relationship between runoff discharge and sediment yield under various flow magnitudes; that is, a high flow rate yielded the most sediment. Fig. 13 shows the general relationship between the two

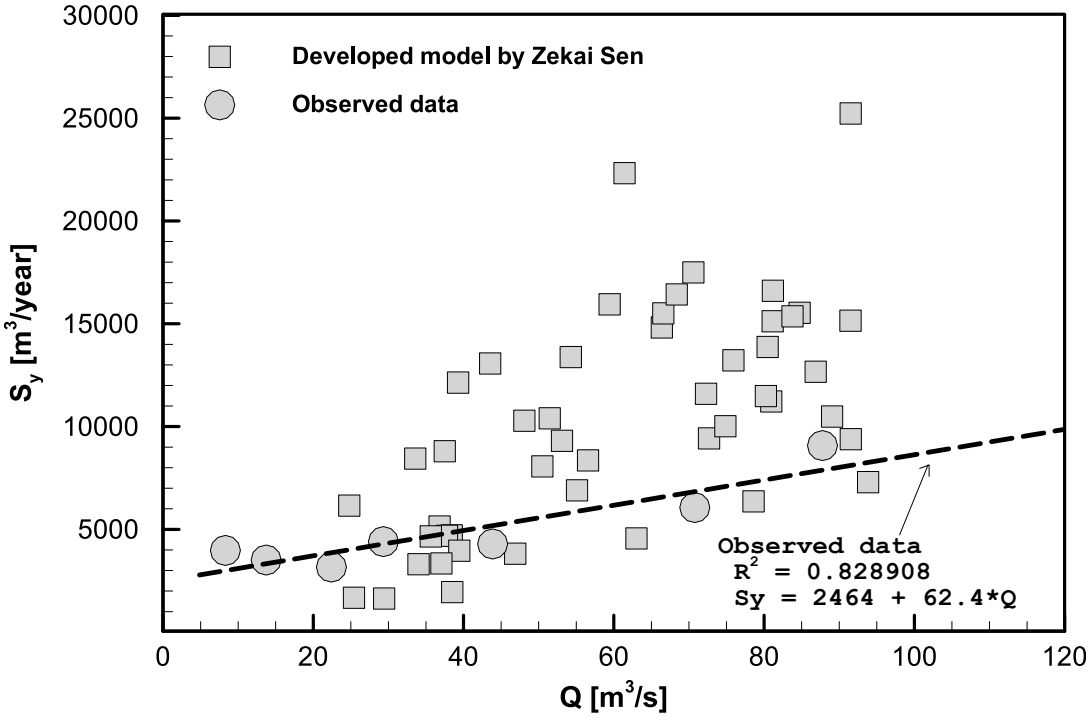

Fig. 13. Sediment yield–runoff relationship between two datasets, developed model by Zekai Şen and observed data (Wadi Assarin).

combined datasets, the equation developed by Şen (2014) and the observed data in Wadi Assarin, to determine the influence of runoff on sediment yield. The observed data trend demonstrates a similar pattern to the developed equation values. However, this trend is supported by the regular drainage basin size and slope. The variations in the eroded sediment volumes from the watershed with runoff discharges can be explained by the rainfall erosivity factor that increases with an increase in intensity and flow rate.

5.3. Sediment yield monitoring techniques

The performance of the digital photogrammetry was validated using point data collected from the 19 sediment scale bars measured in the field using the analysis tools in Agisoft Photoscan. The average RMSEs were approximately 8 and 6 mm for the GCP z-axes in March 2019 and August 2019, respectively; these errors could not be considered purely white noise, and the correlation was thus modelled empirically. Each flight required approximately 2.5 hr for the survey, and data post-processing took almost 12 hr. The two flights were performed at an average flight altitude of 80 m. This research demonstrates that combining digital photogrammetry with UAV reconnaissance is a fast and inexpensive way to retrieve the data needed for these applications.

Nevertheless, the method utilized herein suffers from some problems. First and foremost, from a regulatory point of view, the ordinances regarding the flying of drones are becoming increasingly restrictive, and special authorization is often needed; in fact, piloting a UAV requires a special flying licence in many countries. Moreover, the orography of the surveyed area could represent a further limitation.

Despite these drawbacks, the main advantages of drone surveys over traditional topographic surveys become quite evident during the surveying phase: drone surveys are faster, less expensive, and less laborious. From a hydrological point of view, sedimentation represents a vital issue for dry reservoirs since it reduces the regulation capacities and volumes of reservoirs. Thus, calculating the volume of trapped sediment is necessary for restoring the capacity of a reservoir and financially planning for dam maintenance. The volume of trapped sediment was estimated to be approximately 9075 m^3, representing approximately 1.26 % of the total reservoir capacity. This computed volume was validated using the data observed from the monitored sediment scale bars within the Assarin Dam reservoir, resulting in a 79 % accuracy. These insights, which can support reservoir sustainability and sediment management research, indicate that photogrammetric techniques utilizing UAV-derived imagery represent a suitable solution for determining the volume of trapped sediment within a reservoir.

6. Conclusion

This study assesses reservoir sedimentation in arid region (Wadi Assarin, Oman) and analyses the average soil losses at the catchment scale by combining various methodological approaches based on advanced monitoring techniques and hydrological and empirical models. The proposed relationship between the spatial distribution of soil loss at the catchment scale and trapped sediment in a dam reservoir is presented. The RUSLE method has shown potential for predicting soil loss in wadi systems using a GIS environment and satellite remote sensing data. The total estimated soil loss according to the RUSLE was 196,599 ton/ha yr^{-1}. The rainfall erosivity and topography pattern were matched with the soil loss distribution in the target catchment. The spatial–temporal variability in rainfall patterns and the corresponding runoff discharges lead to high sediment delivery at the outlet of the basin. In addition, we calculated the volume of trapped sediment in a dry reservoir (the Assarin Dam reservoir, located outside Muscat, Oman) using data from two UAV-based photogrammetric field surveys conducted on 17 March 2019 and 25 August 2019, before and after a flash flood event, respectively. The trapped sediment volume was estimated to be approximately 9,075 m^3, representing approximately 1.26 % of the total reservoir capacity; in comparison, interpolation yielded a value of 10829 m^3 with caveats. This volume represents approximately 5.8 % of the total eroded sediment lost from the catchment area. The SDR results for the seven events ranged from 2 % to 5.8 %. The sediment yield from Wadi Assarin generally increased as runoff discharge increased, with the model developed by Şen (2014) and observed datasets matching both degrees and trends. In the MENA region, most of the basins are ungauged; therefore, the adoption of a statistical model and investigation are important to understand the soil erosion and sedimentation processes.

CRediT authorship contribution statement

Mahmood M. Al-mamari: Writing – original draft, Methodology, Software, Validation, Investigation, Visualization. **Sameh A. Kantoush:** Supervision, Conceptualization, Writing – review & editin. **Tahani M. Al-harrasi:** Conceptualization, Data curation, Writing – review & editing. **Ali Al-Maktoumi:** Supervision. **Karim I. Abdrabo:** Writing – review & editing. **Mohamed Saber:** Data curation, Investigation. **Tetsuya Sumi:** Supervision, Project administration.

Declaration of Competing Interest

The authors declare that they have no known competing financial interests or personal relationships that could have appeared to influence the work reported in this paper.

Data availability

Data will be made available on request.

Acknowledgements

This study was supported by the JSPS KAKENHI (Grant Number JP21H01434), JSPS KAKENHI Grant Number 20KK0094, and JSPS Core-to-Core Program Grant Number JPJSCCB20220004. The authors appreciate the Ministry of Agriculture, Fisheries and Water Resources and Sultan Qaboos University, Oman, for supporting the collection of data and information for the Assarin dam reservoir. Additionally, three anonymous reviewers considerably developed the manuscript with American Journal Experts edited English.

References

Abdel-Fattah, Mohammed, Sameh Ahmed Kantoush, Mohamed Saber, and Tetsuya Sumi. 2016. "Hydrological Modelling of Flash Flood at Wadi Samail, Oman." 10.13140/RG.2.2.23353.01126.

Adongo, T.A., Kyei-Baffour, N., Abagale, F.K., Agyare, W.A., 2020. Assessment of reservoir sedimentation of irrigation dams in Northern Ghana. Lake Reservoir Manage. 36 (1), 87–105. https://doi.org/10.1080/10402381.2019.1659461.

Al-Ismaily, S.S., Al-Maktoumi, A.K., Kacimov, A.R., Al-Saqri, S.M., Al-Busaidi, H.A., Al-Haddabi, M.H., 2013. Morphed block-crack preferential sedimentation in a reservoir bed: a smart design and evolution in nature. Hydrol. Sci. J. 58 (8), 1779–1788. https://doi.org/10.1080/02626667.2013.838002.

Allafta, H., Opp, C., 2022. Soil erosion assessment using the RUSLE model, remote sensing, and GIS in the Shatt Al-Arab Basin (Iraq-Iran). Appl. Sci. 12 (15), 7776. https://doi.org/10.3390/app12157776.

Al-mamari, M., Kantoush, S., Kobayashi, S., Sumi, T., Saber, M., 2019. Real-time measurement of flash-flood in a Wadi Area by LSPIV and STIV. Hydrology 6 (1), 27. https://doi.org/10.3390/hydrology6010027.

Al-Saqri, S., Al-Maktoumi, A., Al-Ismaily, S., Kacimov, A., Al-Busaidi, H., 2016. Hydropedology and soil evolution in explaining the hydrological properties of recharge dams in arid zone environments. Arab. J. Geosci. 9 (1), 47. https://doi.org/10.1007/s12517-015-2076-0.

Arseni, V., Georgescu, I., Rosu., 2019. Testing different interpolation methods based on single beam echosounder river surveying. case study: Siret River. ISPRS Int. J. Geo Inf. 8 (11), 507. https://doi.org/10.3390/ijgi8110507.

Asthana, B.N., Khare, D., 2022. Recent Advances in Dam Engineering. Springer International Publishing, Cham.

Azab, Y.F.A., Abbas, H.H., Jalhoum, M.E.M., Farid, I.M., Abdelhameed, A.-E., Mohamed, E.S., 2021. Soil erosion assessment in arid region: a case study in Wadi Naghamish, Northwest Coast, Egypt. Egypt. J. Remote Sens. Space Sci. S1110982321000946 https://doi.org/10.1016/j.ejrs.2021.11.008.

Borrelli, P., Alewell, C., Alvarez, P., Anache, J.A.A., Baartman, J., Ballabio, C., Bezak, N., Biddoccu, M., Cerdà, A., Chalise, D., Chen, S., Chen, W., Girolamo, A.M.D., Gessesse, G.D., Deumlich, D., Diodato, N., Efthimiou, N., Erpul, G., Fiener, P., Freppaz, M., Gentile, F., Gericke, A., Haregeweyn, N., Bifeng, H.u., Jeanneau, A., Kaffas, K., Kiani-Harchegani, M., Villuendas, I.L., Li, C., Lombardo, L., López-Vicente, M., Lucas-Borja, M.E., Märker, M., Matthews, F., Miao, C., Mikoš, M., Modugno, S., Möller, M., Naipal, V., Nearing, M., Owusu, S., Panday, D., Patault, E., Patriche, C.V., Poggio, L., Portes, R., Quijano, L., Rahdari, M.R., Renima, M., Ricci, G.F., Rodrigo-Comino, J., Saia, S., Samani, A.N., Schillaci, C., Syrris, V., Kim, H.S., Spinola, D.N., Oliveira, P.T., Teng, H., Thapa, R., Vantas, K., Vieira, D., Yang, J.E., Yin, S., Zema, D.A., Zhao, G., Panagos, P., 2021. Soil erosion modelling: a global review and statistical analysis. Sci. Total Environ. 780, 146494 https://doi.org/10.1016/j.scitotenv.2021.146494.

Brune, G.M., 1953. Trap efficiency of reservoirs. Trans. Am. Geophys. Union 34 (3), 407. https://doi.org/10.1029/TR034i003p00407.

Bulti, A.T., 2021. The influence of dam construction on the catchment hydrologic behaviour and its effects on a discharge forecast in hydrological models. Water Resour. Manag. 35 (6), 2023–2037. https://doi.org/10.1007/s11269-021-02829-z.

Cândido, B.M., Quinton, J.N., James, M.R., Silva, M.L.N., de Carvalho, T.S., de Lima, W., Beniaich, A., Eltner, A., 2020. High-resolution monitoring of diffuse (sheet or interrill) erosion using structure-from-motion. Geoderma 375, 114477. https://doi.org/10.1016/j.geoderma.2020.114477.

Clapuyt, F., Vanacker, V., Van Oost, K., 2016. Reproducibility of UAV-based earth topography reconstructions based on structure-from-motion algorithms. Geomorphology 260, 4–15.

Cook, Howard L. 1937. "The Nature and Controlling Variables of the Water Erosion Process.".

Durigon, V.L., Carvalho, D.F., Antunes, M.A.H., Oliveira, P.T.S., Fernandes, M.M., 2014. NDVI time series for monitoring RUSLE cover management factor in a tropical watershed. Int. J. Remote Sens. 35 (2), 441–453. https://doi.org/10.1080/01431161.2013.871081.

Dutta, S., 2016. Soil erosion, sediment yield and sedimentation of reservoir: a review. Model. Earth Syst. Environ. 2 (3), 123. https://doi.org/10.1007/s40808-016-0182-y.

Eini, M.R., Olyaei, M.A., Kamyab, T., Teymoori, J., Brocca, L., Piniewski, M., 2021. Evaluating three non-gauge-corrected satellite precipitation estimates by a regional gauge interpolated dataset over Iran. J. Hydrol.: Reg. Stud. 38, 100942.

Elçi, Ş., Work, P.A., Hayter, E.J., 2007. Influence of stratification and shoreline erosion on reservoir sedimentation patterns. J. Hydraul. Eng. 133 (3), 255–266. https://doi.org/10.1061/(ASCE)0733-9429(2007)133:3(255).

Elhag, M., Hidayatulloh, A., Bahrawi, J., Chaabani, A., Budiman, J., 2022. Using inconsistencies of wadi morphometric parameters to understand patterns of soil erosion. Arab. J. Geosci. 15 (14), 1299. https://doi.org/10.1007/s12517-022-10422-w.

Elnashar, A., Zeng, H., Bingfang, W.u., Fenta, A.A., Nabil, M., Duerler, R., 2021. Soil erosion assessment in the blue nile basin driven by a novel RUSLE-GEE Framework. Sci. Total Environ. 793, 148466 https://doi.org/10.1016/j.scitotenv.2021.148466.

Eniyew, S., Teshome, M., Sisay, E., Bezabih, T., 2021. Integrating RUSLE model with remote sensing and GIS for evaluation soil erosion in Telkwonz Watershed, Northwestern Ethiopia. Remote Sens. Appl.: Soc. Environ. 24, 100623.

Farhan, Y., Nawaiseh, S., 2015. Spatial assessment of soil erosion risk using RUSLE and GIS techniques. Environ. Earth Sci. 74 (6), 4649–4669. https://doi.org/10.1007/s12665-015-4430-7.

Gaubi, I., Chaabani, A., Ben Mammou, A., Hamza, M.H., 2017. A GIS-based soil erosion prediction using the revised universal soil loss equation (RUSLE)(Lebna Watershed, Cap Bon, Tunisia). Nat. Hazards 86 (1), 219–239.

George, M.W., Hotchkiss, R.H., Huffaker, R., 2017. Reservoir sustainability and sediment management. J. Water Resour. Plan. Manag. 143 (3), 04016077. https://doi.org/10.1061/(ASCE)WR.1943-5452.0000720.

Ghernaout, R., Remini, B., 2014. Impact of suspended sediment load on the silting of SMBA reservoir (Algeria). Environ. Earth Sci. 72 (3), 915–929. https://doi.org/10.1007/s12665-014-3125-9.

GUERRA, Antônio José Teixeira, Michael Augustine Fullen, Maria do Carmo Oliveira JORGE, José Fernando Rodrigues BEZERRA, and Mohamed S. Shokr. 2017. "Slope Processes, Mass Movement and Soil Erosion: A Review." *Pedosphere* 27(1):27–41.

Hengl, T., Mendes, J., de Jesus, G.B.M., Heuvelink, M.R., Gonzalez, M.K., Blagotić, A., Shangguan, W., Wright, M.N., Geng, X., Bauer-Marschallinger, B., Guevara, M.A., Vargas, R., MacMillan, R.A., Batjes, N.H., Leenaars, J.G.B., Ribeiro, E., Wheeler, I., Mantel, S., Kempen, B., 2017. SoilGrids250m: global gridded soil information based on machine learning. PLoS One 12 (2), e0169748.

ICOLD, 2009. Sedimentation and Sustainable Use of Reservoirs and River Systems. International Commission on Large Dams (ICOLD), Paris.

Islam, Z., 2022. Soil loss assessment by RUSLE in the cloud-based platform (GEE) in Nigeria. Model. Earth Syst. Environ. 1–13.

Kantoush, SamehA, Mahmood M. Al-mamari, Tahani Al-harrasi, Mohamed Saber, and Tetsuya Sumi. 2022. "Estimating Sediment Yield and Morphological Changes in Dry Reservoirs: Case Study Wadi Assarin, Oman." 7.

Kirurhika, A.M., Arunachalam, S., Reddy, A.K., Suresh, S.B., 2011. Silt sediment analysis for devarabelekere reservoir using remote sensing and GIS. Int J Earth Sci Eng 4 (1), 24–30.

Kulimushi, L.C., Choudhari, P., Mubalama, L.K., Banswe, G.T., 2021. GIS and remote sensing-based assessment of soil erosion risk using RUSLE model in South-Kivu Province, Eastern, Democratic Republic of Congo. Geomat. Nat. Haz. Risk 12 (1), 961–987.

Malmon, D.V., Reneau, S.L., Katzman, D., Lavine, A., Lyman, J., 2007. Suspended sediment transport in an ephemeral stream following wildfire. J. Geophys. Res. 112 (F2), F02006. https://doi.org/10.1029/2005JF000459.

Melalih, A., Mazour, M., 2021. Analysis of water and soil conservation techniques at the Ain Sefra Arid watershed (Ksour Mountains, Southwest Algeria). Environ. Monit. Assess. 193 (1), 33. https://doi.org/10.1007/s10661-020-08842-w.

Ministry of Regional Municipalities & Water Resources. 2012. *Dams in Oman*. 5.

Miranda, M.N., 2021. Sedimentation assessment and effects in Venda Nova Dam Reservoir (Portugal). Sci. Total Environ. 11.

Moore, I.D., Grayson, R.B., Ladson, A.R., 1991. Digital Terrain modelling: a review of hydrological, geomorphological, and biological applications. Hydrol. Process. 5 (1), 3–30. https://doi.org/10.1002/hyp.3360050103.

Moraetis, D., Scharf, A., Mattern, F., Pavlopoulos, K., Forman, S., 2020. Quaternary thrusting in the central oman mountains—novel observations and causes: insights from optical stimulate luminescence dating and kinematic fault analyses. Geosciences 10 (5), 166. https://doi.org/10.3390/geosciences10050166.

Nesbit, P., Hugenholtz, C., 2019. Enhancing UAV–SfM 3D model accuracy in high-relief landscapes by incorporating oblique images. Remote Sens. (Basel) 11 (3), 239. https://doi.org/10.3390/rs11030239.

Ostovari, Y., Moosavi, A.A., Mozaffari, H., Poppiel, R.R., Tayebi, M., Demattê, J.AM., 2022. Soil Erodibility and Its Influential Factors in the Middle East. In: Computers in Earth and Environmental Sciences. Elsevier, pp. 441–454.

Özcan, O., Özcan, O., 2021. Multi-temporal UAV based repeat monitoring of rivers sensitive to flood. J. Maps 17 (3), 163–170. https://doi.org/10.1080/17445647.2020.1820387.

Polat, N., Uysal, M., Toprak, A.S., 2015. An investigation of DEM generation process based on LiDAR data filtering, decimation, and interpolation methods for an urban area. Measurement 75, 50–56. https://doi.org/10.1016/j.measurement.2015.08.008.

Prathapar, S.A., Bawain, A.A., 2014. Impact of sedimentation on groundwater recharge at Sahalanowt Dam, Salalah, Oman. Water Int. 39 (3), 381–393. https://doi.org/10.1080/02508060.2014.895889.

Renard, K.G., 1997. Predicting Soil Erosion by Water: A Guide to Conservation Planning with the Revised Universal Soil Loss Equation (RUSLE). United States Government Printing.

Renard, K. G., and L. J. Lane. n.d. "SEDIMENT YIELD AS RELATED TO A STOCHASTIC MODEL OF EPHEMERAL RUNOFF." 11.

Rishikeshan, C.A., Katiyar, S.K., Vishnu Mahesh, V.N., 2014. Detailed Evaluation of DEM Interpolation Methods in GIS Using DGPS Data. In: In *2014 International Conference on Computational Intelligence and Communication Networks*. IEEE, Bhopal, India, pp. 666–671.

Rogers, S.R., Manning, I., Livingstone, W., 2020. Comparing the spatial accuracy of digital surface models from four unoccupied aerial systems: photogrammetry versus LiDAR. Remote Sens. (Basel) 12 (17), 2806. https://doi.org/10.3390/rs12172806.

Saber, Mohamed, Sameh Kantoush, Tetsuya Sumi, and Yusuke Ogiso. 2019. "Reservoir Sedimentation at Wadi System: Challenges and Management Strategies." *京都大学防災研究所年報. B* 62(B):689–99.

Salach, A., Bakuła, K., Pilarska, M., Ostrowski, W., Górski, K., Kurczyński, Z., 2018. Accuracy assessment of point clouds from LiDAR and dense image matching acquired using the UAV platform for DTM creation. ISPRS Int. J. Geo Inf. 7 (9), 342.

Şen, Z., 2014. Sediment yield estimation formulations for arid regions. Arab. J. Geosci. 7 (4), 1627–1636.

Sharpley, Andrew N., and Jimmy R. Williams. 1990. "EPIC-Erosion/Productivity Impact Calculator. I: Model Documentation. II: User Manual." *Technical Bulletin-United States Department of Agriculture* (1768).

Shiferaw, M., Abebe, R., 2021. Reservoir sedimentation and estimating dam storage capacity using bathymetry survey: a case study of Abrajit Dam, Upper Blue Nile Basin, Ethiopia. Applied Geomatics 13 (3), 277–286. https://doi.org/10.1007/s12518-020-00348-x.

Tamminga, A.D., Eaton, B.C., Hugenholtz, C.H., 2015. UAS-based remote sensing of fluvial change following an extreme flood event: UAS remote sensing of flood effects. Earth Surf. Proc. Land. 40 (11), 1464–1476. https://doi.org/10.1002/esp.3728.

Tebbi, F.Z., Dridi, H., Morris, G.L., 2012. Optimization of cumulative trapped sediment curve for an arid zone reservoir: Foum El Kherza (Biskra, Algeria). Hydrol. Sci. J. 57 (7), 1368–1377. https://doi.org/10.1080/02626667.2012.712740.

Tinkham, W.T., Swayze, N.C., 2021. Influence of Agisoft metashape parameters on UAS structure from motion individual tree detection from canopy height models. Forests 12 (2), 250. https://doi.org/10.3390/f12020250.

Tsunetaka, H., Hotta, N., Hayakawa, Y.S., Imaizumi, F., 2020. Spatial Accuracy Assessment of Unmanned Aerial Vehicle-Based Structures from Motion Multi-View Stereo Photogrammetry for Geomorphic Observations in Initiation Zones of Debris Flows, Ohya Landslide, Japan. Prog Earth Planet Sci 7 (1), 24. https://doi.org/10.1186/s40645-020-00336-0.

Wang, H., Zhao, H.u., 2020. Dynamic Changes of Soil Erosion in the Taohe River Basin Using the RUSLE Model and Google Earth Engine. Water 12 (5), 1293.

Wasson, R. J. 1994. "Annual and Decadal Variation of Sediment Yield in Australia, and Some Global Comparisons." 11.

Wheaton, J.M., Brasington, J., Darby, S.E., Sear, D.A., 2009. Accounting for Uncertainty in DEMs from Repeat Topographic Surveys: Improved Sediment Budgets. *Earth Surf. Proc. Land.* n/a-n/a. https://doi.org/10.1002/esp.1886.

Wischmeier, W.H., Smith, D.D., 1978. Predicting Rainfall Erosion Losses: A Guide to Conservation Planning. Department of Agriculture, Science and Education Administration.

Yousefi, S., Pourghasemi, H.R., Rahmati, O., Keesstra, S., Emami, S.N., Hooke, J., 2021. Geomorphological Change Detection of an Urban Meander Loop Caused by an Extreme Flood Using Remote Sensing and Bathymetry Measurements (a Case Study of Karoon River, Iran). J. Hydrol. 597, 125712 https://doi.org/10.1016/j.jhydrol.2020.125712.

Ziadat, F.M., Taimeh, A.Y., 2013. Effect of rainfall intensity, slope, land use and antecedent soil moisture on soil erosion in an arid environment: factors affecting soil erosion in an arid environment. Land Degrad. Dev. 24 (6), 582–590. https://doi.org/10.1002/ldr.2239.